THE EXTENDED H_∞ FILTER FOR CALIBRATION AND ATTITUDE DETERMINATION USING REAL DATA OF CBERS-2 SATELLITE

W. R. Silva[1], H. K. Kuga[1], and M. C. Zanardi[2]

[1]*Space Mechanics and Control Division, National Institute for Space Research (INPE), Av dos Astronautas, 1758, Jd. da Granja, CEP:12227-010, São José dos Campos, S.P., Brazil. E-mails: reis.william@gmail.com, helio.kuga@inpe.br*

[2]*Universidade Federal do ABC (UFABC), Av. dos Estados, 5001, Bangu, CEP:09210-580, Santo André, S.P., Brazil. E-mail: mceciliazanardi@gmail.com*

Abstract: *This work describes the attitude and the gyros drift estimation for real satellite CBERS-2 (China Brazil Earth Resources Satellite 2) using the Second-Order Extended H_∞ Filter for nonlinear systems. The attitude dynamical model is described by nonlinear equations involving the Euler angles. The attitude sensors available are two DSS (Digital Sun Sensors), two IRES (Infra-Red Earth Sensor), and one triad of mechanical gyros. The two IRES give direct measurements of roll and pitch angles with a certain level of error. The two DSS are mounted on the satellite body such that they are nonlinear functions of roll, pitch, and yaw attitude angles. Herein one proposes to use an extension of the H_∞ linear filter for the nonlinear case of attitude estimation with nonlinearity in both the dynamics and the measurement model. The aim is to highlight and magnify the properties of the H_∞ filter in terms of its favourable characteristics. The results in this work show that one can reach accuracies in attitude determination within the prescribed requirements, besides providing estimates of the gyro drifts which can be further used to enhance the gyro error model and that the Second-Order Extended H_∞ Filter is more robust than Extended Kalman Filter.*

Keywords: *Second-Order Extended H_∞ Filter, Extended Kalman Filter, nonlinear system, attitude estimation, gyros drift.*

1. Introduction

Attitude estimation is a process of determining the orientation of a satellite with respect to an inertial reference system by processing data from attitude sensors. Given a reference vector, the attitude sensor measures the orientation of this vector with respect to the satellite system. Then, it is possible to estimate the orientation of the satellite processing computationally these vectors using attitude estimation methods.

In this work the attitude is represented by Euler angles, due to its easy geometrical interpretation. In the case of CBERS-2 (China-Brazil Earth Resources Satellite), the attitude stabilization is done in three axes namely geo-targeted, and can be described in relation to the orbital system. In this frame, the movement around the direction of the orbital speed is named *roll* (ϕ), the movement around the direction normal to the orbit is called *pitch* (θ), and finally the movement around the Zenith/Nadir direction is called *yaw* (ψ). See Fig. 1.

The state estimation process was performed by the Second-Order Extended H_∞ Filter. This method is capable of estimating nonlinear systems states from data obtained from different sensors of attitude. It was considered real data supplied by gyroscopes, infrared Earth sensors and digital sun
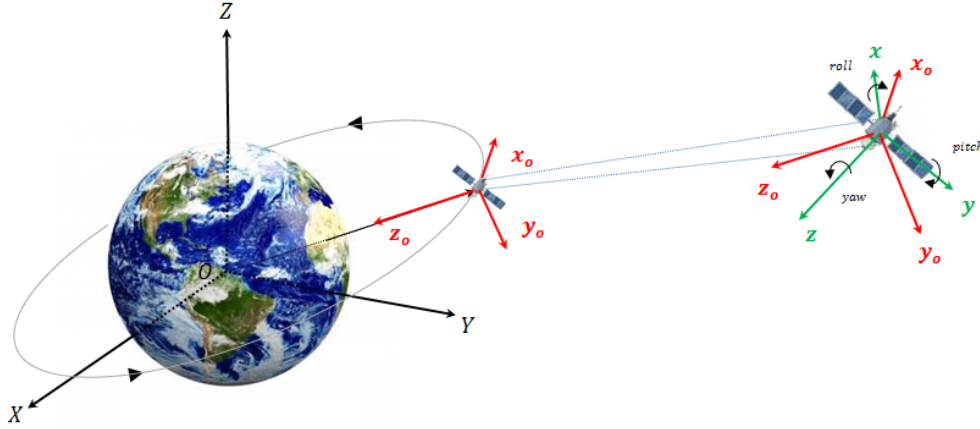
Figure 1. The orbital local system $(\mathbf{x}_o, \mathbf{y}_o, \mathbf{z}_o)$ and the attitude system $(\mathbf{x}, \mathbf{y}, \mathbf{z})$

sensors. These sensors are on board the CBERS-2 satellite, and the measurements were recorded by the Satellite Control Center of INPE (Brazilian Institute for Space Research).

The H_∞ filtering minimizes the worst-case estimation error and is thus more robust than conventional Kalman filtering. The H_∞ Filter is based on the game theory approach that was originally developed by Reference [1] and is further discussed in References [2] and [3]. The extended form is discussed in Reference [4]. In this game theory approach, the designer prepares for the worst strategy that the nature can provide. Therefore, the state estimator and the signal disturbance (initial condition error, process noise and measurements noise) have conflicting objectives, which are to mininize and maximize the estimation error respectively. The estimation criterion in the H_∞ filter design is to minimize the worst possible effects of the disturbance signals on the signal estimation error without *a priori* knowledge of them.

2. Attitude Representation by Euler Angles

The attitude of a satellite is defined by a set of parameters that allow, uniquely correlating in an instant of time, a fixed coordinate system of the satellite (which accompanies his movement of rotation and translation) to another inertial system, which is usually related to the Earth [5].

In general it is considered inertial or near-inertial, which means that its movement in relation to the system truly inertial is despicable, when compared with the movement of the body itself. A way to represent the attitude is by Euler angles, which will express the relationship between two coordinate systems, one of them fixed on satellite and other associated to an inertial system.

As previously mentioned, the movement around the direction of the orbital speed is named *roll* (ϕ), the movement around the direction normal to the orbit is called *pitch* (θ), and the movement around the Zenith/Nadir direction is called *yaw* (ψ). See Fig. 2.

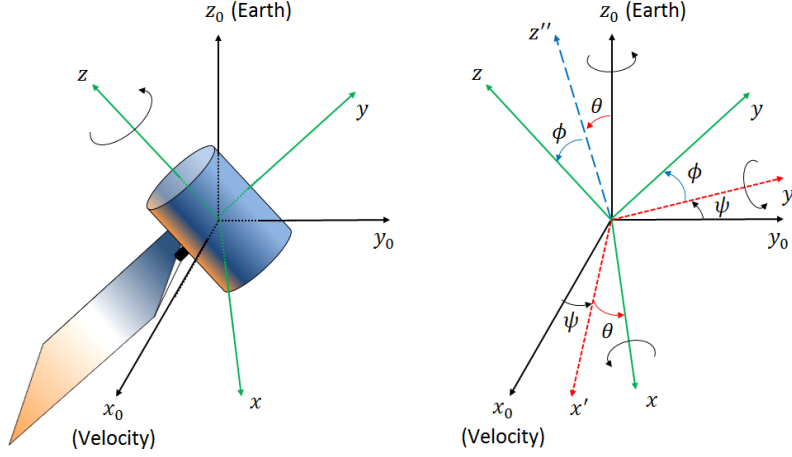The transformation matrix R, which relates the fixed coordinate system in the satellite's body $(\mathbf{x}, \mathbf{y}, \mathbf{z})$

2

Figure 2. The rotation sequence adopted (ϕ, θ, ψ)

with the orbital coordinate system $(\mathbf{x}_o, \mathbf{y}_o, \mathbf{z}_o)$, has its elements described in terms of Euler angles (ϕ, θ, ψ). The rotation sequence adopted in this work was the 3-2-1, and the following sequences of rotations are used [6]

- 1st rotation of an angle ψ (*yaw* angle) around the $\mathbf{z}_o$ axis.
- 2nd rotation of an angle θ (*pitch* angle) around an intermediate $\mathbf{y}'$ axis.
- 3rd rotation of an angle ϕ (*roll* angle) around the $\mathbf{x}$ axis.

Thus, we have that:

$$R = \begin{bmatrix} \cos\theta\cos\psi & \cos\theta\sin\psi & -\sin\theta \\ \sin\phi\sin\theta\cos\psi - \sin\psi\cos\phi & \sin\phi\sin\theta\sin\psi + \cos\phi\cos\psi & \sin\phi\cos\theta \\ \cos\phi\sin\theta\cos\psi + \sin\phi\sin\psi & \cos\phi\sin\theta\sin\psi - \sin\phi\cos\psi & \cos\phi\cos\theta \end{bmatrix} \quad (1)$$

In turn, the kinematic equations of Euler angles are given by [6, 7]:

$$\begin{bmatrix} \dot{\phi} \\ \dot{\theta} \\ \dot{\psi} \end{bmatrix} = \begin{bmatrix} 1 & \sin\phi\tan\theta & \cos\phi\tan\theta \\ 0 & \cos\phi & -\sin\phi \\ 0 & \sin\phi\sec\theta & \cos\phi\sec\theta \end{bmatrix} \begin{bmatrix} \omega_x \\ \omega_y \\ \omega_z \end{bmatrix} \quad (2)$$

where, ω_x, ω_y and ω_z are the components of the angular velocity of the satellite in *roll*, *pitch* e *yaw* directions.

By representing the attitude of a satellite with Euler angles, the set of kinematic equations are given by [6, 8]:

$$\begin{bmatrix} \dot{\phi} \\ \dot{\theta} \\ \dot{\psi} \end{bmatrix} = \begin{bmatrix} 1 & \sin\phi\tan\theta & \cos\phi\tan\theta \\ 0 & \cos\phi & -\sin\phi \\ 0 & \sin\phi\sec\theta & \cos\phi\sec\theta \end{bmatrix} \left\{ \begin{bmatrix} \hat{\omega}_x \\ \hat{\omega}_y \\ \hat{\omega}_z \end{bmatrix} - R \begin{bmatrix} 0 \\ \omega_0 \\ 0 \end{bmatrix} \right\} \quad (3)$$

where ω_0 is the orbital angular velocity; $(\hat{\omega}_x, \hat{\omega}_y, \hat{\omega}_z)$ are the components of the angular velocity of the satellite on the satellite system axes.

Defining the state vector composed by: Euler angles (ϕ, θ, ψ) and the components of the gyros bias $(\varepsilon_x, \varepsilon_y, \varepsilon_x)$; and assuming that ϕ and θ are small angles, the differential equations of state for attitude and bias of the gyros are modeled as follows [8, 9]:

$$
\begin{aligned}
\dot{\phi} &= \omega_0 \sin \psi + \hat{\omega}_x + \theta \hat{\omega}_z \\
\dot{\theta} &= \omega_0 \cos \psi + \hat{\omega}_y - \phi \hat{\omega}_z \\
\dot{\psi} &= \omega_0 \theta \sin \psi + \hat{\omega}_z + \phi \hat{\omega}_y \\
\dot{\varepsilon}_x &= 0 \\
\dot{\varepsilon}_y &= 0 \\
\dot{\varepsilon}_z &= 0
\end{aligned}
\tag{4}
$$

where ϕ, θ and ψ are the attitude angles obtained by some estimation process, and $\hat{\omega}_i$ are the gyros measurements.

3. Mathematical Models of Attitude Sensors

In order to ascertain the attitude of an artificial satellite it is necessary to use some attitude sensors. In this section is described the mathematical model of the attitude sensors used in this research for the determination of attitude: gyros, digital sun sensor and infrared Earth sensor.

3.1. Mathematical Model of Gyroscope

The main advantage of using gyros is that they can provide the angular displacement and/or the angular velocity of the satellite directly. The mechanical gyro has a wheel that rotates at high speed that responds to changes in the inertial guidance of its axis of rotation which it is aligned to the axis of rotation of the satellite.

In this work the gyros (*Rate Integration Gyros-RIG's*) are used to measure the angular velocity of roll, pitch and yaw axes of the satellite. In addition, the drift errors (bias), due to minor imperfections of its mechanism, are included in the State vector to be estimated. The RIG's model is given by [7]:

$$
\Delta \boldsymbol{\Theta}_i = \int_0^{\Delta t} (\boldsymbol{\omega}_i + \boldsymbol{\varepsilon}_i) \, dt, \qquad (i = x, y, z)
\tag{5}
$$

where, $\Delta \boldsymbol{\Theta}_i$ are the angular displacements measured in the axes of the satellite in a time interval Δt, $\boldsymbol{\omega}_i$ are the components of the angular velocity of the satellite system and $\boldsymbol{\varepsilon}_i$ are the components of the gyro bias.

The measurement of the components of the angular velocity of the satellite is represented as:

$$
\hat{\boldsymbol{\omega}}_i = \frac{d\boldsymbol{\Theta}_i}{dt} - \hat{\boldsymbol{\varepsilon}}_i - \boldsymbol{\eta}_i = \boldsymbol{g}_i - \hat{\boldsymbol{\varepsilon}}_i - \boldsymbol{\eta}_i
\tag{6}
$$

where, $\boldsymbol{g}_i(t)$ is the gyro output vector and $\boldsymbol{\eta}_i(t)$ is the white Gaussian noise process, which covers all remaining non-modeled effects besides the random noises.

3.2. Mathematical Model of Infrared Earth Sensor

The horizon Sensor is an optical instrument used to detect the light emitted by the edge of the Earth's atmosphere. Infrared sensors are used to detect the heat from the Earth's atmosphere, which is very hot compared to the cold of space, thus they are called Infrared Earth Sensors(IRES). The IRES determine the angle between the direction of an axis of symmetry of the satellite and the direction from the center of the Earth.

When using the IRES, it may help to estimate drift errors present in gyro [10, 11]. In this work, two sensors are used, where one measures the *roll* angle and the other measures the *pitch* angle.

The equations of measurements for Infrared Earth Sensors (IRES) are given by [6].

$$\phi_H = \phi + \upsilon_{\phi_H}$$
$$\theta_H = \theta + \upsilon_{\theta_H} \tag{7}$$

where υ_{ϕ_H} and υ_{θ_H} are the white noise that represent small remaining effects of misalignment during installation and/or by assembly of sensor. These errors are assumed Gaussian ones.

3.3. Mathematical Model of Digital Sun Sensor

The Digital Sun Sensor is an optical device that detects the Sun and sets the position of one of the main axes of symmetry of the spacecraft relative to the direction in which the Sun was detected. The Digital Sun Sensor (DSS) of the CBERS-2 is not able to measure the *yaw* angle, *i.e.*, these sensors do not provide direct measures, it measures the coupled *pitch* angle (α_θ) and *yaw* angle (α_ψ). The equations of measurements for the Digital Sun Sensors (DSS) are obtained as follows [6, 8].

$$\alpha_\psi = \arctan\left(\frac{-S_y}{S_x \cos 60° + S_z \cos 150°}\right) + \upsilon_{\alpha_\psi} \tag{8}$$

when $|S_x \cos 60° + S_z \cos 150°| \geq \cos 60°$, and

$$\alpha_\theta = 24° + \arctan\left(\frac{S_x}{S_z}\right) + \upsilon_{\alpha_\theta} \tag{9}$$

when $\left|24° + \arctan\left(\frac{S_x}{S_z}\right)\right| < 60°$, where υ_{α_ψ} and υ_{α_θ} are the white noise and represent small effects remnants of misalignment during installation and/or by sensor assembly. Just as the Infrared Earth Sensor, these errors are assumed Gaussian ones.

The conditions must be such that the solar vector is in the field of sight of sensor and S_x, S_y, S_z are the components of the unit vector associated with the solar vector satellite system at date by:

$$S_x = S_{0x} + \psi S_{0y} - \theta S_{0z}$$
$$S_y = S_{0y} - \psi S_{0x} + \phi S_{0z} \tag{10}$$
$$S_z = S_{0z} - \phi S_{0y} - \theta S_{0z}$$

where S_{0x}, S_{0y} e S_{0z} are the components of the solar vector in orbital coordinate system [6] and ϕ, θ e ψ are the Euler angles, which represent the estimated attitude.

4. Problem Formulation for the Second-Order Extended H_∞ Filter

Consider a nonlinear discrete time system

$$\begin{aligned}
\boldsymbol{x}_{k+1} &= f(\boldsymbol{x}_k, \boldsymbol{u}_k) + \boldsymbol{w}_k \\
\boldsymbol{y}_k &= h(\boldsymbol{x}_k) + \boldsymbol{v}_k
\end{aligned} \tag{11}$$

where k is the discrete time index, $\boldsymbol{x}_{k+1}$ and $\boldsymbol{y}_k$ are the state and measurements vectors with dimensions of n and m respectively, $\boldsymbol{w}_k$ and $\boldsymbol{v}_k$ are process and measurements noises, these noise terms may be random with possibly unknown statistics and nonzero mean, or they may be deterministic. The term $\boldsymbol{u}_k$ is the control input and $f(.)$ and $h(.)$ are vectors of nonlinear functions that are differentiable with respect to $\boldsymbol{x}_k$.

Hence, the second-order Taylor series expansion of $f(\boldsymbol{x}_k, \boldsymbol{u}_k)$ and $h(\boldsymbol{x}_k)$ around the nominal point $\hat{\boldsymbol{x}}_k$ (the estimated state) are

$$f(\boldsymbol{x}_k, \boldsymbol{u}_k) = f(\hat{\boldsymbol{x}}_k, \boldsymbol{u}_k) + \left.\frac{\partial f}{\partial \boldsymbol{x}_k}\right|_{\hat{\boldsymbol{x}}_k} (\boldsymbol{x}_k - \hat{\boldsymbol{x}}_k) + \frac{1}{2}\sum_{i=1}^{n} \varphi_i^f (\boldsymbol{x}_k - \hat{\boldsymbol{x}}_k)^T \left.\frac{\partial^2 f_i}{\partial \boldsymbol{x}_k^2}\right|_{\hat{\boldsymbol{x}}_k} (\boldsymbol{x}_k - \hat{\boldsymbol{x}}_k) \tag{12}$$

$$h(\boldsymbol{x}_k) = h(\hat{\boldsymbol{x}}_k) + \left.\frac{\partial h}{\partial \boldsymbol{x}_k}\right|_{\hat{\boldsymbol{x}}_k} (\boldsymbol{x}_k - \hat{\boldsymbol{x}}_k) + \frac{1}{2}\sum_{i=1}^{m} \varphi_i^h (\boldsymbol{x}_k - \hat{\boldsymbol{x}}_k)^T \left.\frac{\partial^2 h_i}{\partial \boldsymbol{x}_k^2}\right|_{\hat{\boldsymbol{x}}_k} (\boldsymbol{x}_k - \hat{\boldsymbol{x}}_k) \tag{13}$$

where f_i and h_i are the ith element of $f(\boldsymbol{x}_k, \boldsymbol{u}_k)$ and $h(\boldsymbol{x}_k)$, respectively. The terms φ_i^f and φ_i^h are vectors given by $\varphi_i^f = \begin{bmatrix} 0 & \dots & 0 & 1 & 0 & \dots & 0 \end{bmatrix}_{n\times 1}^T$ and $\varphi_i^h = \begin{bmatrix} 0 & \dots & 0 & 1 & 0 & \dots & 0 \end{bmatrix}_{m\times 1}^T$ where the one is in the ith element. The quadratic term in Eq. (12) and (13) can be written as

$$(\boldsymbol{x}_k - \hat{\boldsymbol{x}}_k)^T \left.\frac{\partial^2 f_i}{\partial \boldsymbol{x}_k^2}\right|_{\hat{\boldsymbol{x}}_k} (\boldsymbol{x}_k - \hat{\boldsymbol{x}}_k) = tr\left[\left.\frac{\partial^2 f_i}{\partial \boldsymbol{x}_k^2}\right|_{\hat{\boldsymbol{x}}_k} (\boldsymbol{x}_k - \hat{\boldsymbol{x}}_k)(\boldsymbol{x}_k - \hat{\boldsymbol{x}}_k)^T \right] \approx tr\left[\left.\frac{\partial^2 f_i}{\partial \boldsymbol{x}_k^2}\right|_{\hat{\boldsymbol{x}}_k} \bar{\boldsymbol{P}}_k \right] \tag{14}$$

$$(\boldsymbol{x}_k - \hat{\boldsymbol{x}}_k)^T \left.\frac{\partial^2 h_i}{\partial \boldsymbol{x}_k^2}\right|_{\hat{\boldsymbol{x}}_k} (\boldsymbol{x}_k - \hat{\boldsymbol{x}}_k) = tr\left[\left.\frac{\partial^2 h_i}{\partial \boldsymbol{x}_k^2}\right|_{\hat{\boldsymbol{x}}_k} (\boldsymbol{x}_k - \hat{\boldsymbol{x}}_k)(\boldsymbol{x}_k - \hat{\boldsymbol{x}}_k)^T \right] \approx tr\left[\left.\frac{\partial^2 h_i}{\partial \boldsymbol{x}_k^2}\right|_{\hat{\boldsymbol{x}}_k} \bar{\boldsymbol{P}}_k \right] \tag{15}$$

where $tr[.]$ is the trace operation and it was assumed that the matrix $\bar{\boldsymbol{P}}_k$ can be estimated by the sample covariance matrix of the estimation error.

The goal is to estimate a linear combination of the state. That is, we want to estimate z_k, which is given by

$$z_k = \boldsymbol{L}_k \boldsymbol{x}_k \tag{16}$$

where $\boldsymbol{L}_k$ is a user-defined matrix with full rank. If we want to directly estimate $\boldsymbol{x}_k$ as in the Kalman Filter, then we set $\boldsymbol{L}_k = \boldsymbol{I}$. The estimate of z_k is denoted as $\hat{z}_k$ and the estimate of the initial state $\boldsymbol{x}_0$ is $\hat{\boldsymbol{x}}_0$.

The design criterion for the Second-Order Extended H_∞ Filter is to find $\hat{z}_k$ that minimizes $(z_k - \hat{z}_k)$ for any w_k, v_k and x_0. Considering the worst-case scenario, assuming that the nature is our adversary one needs to find w_k, v_k and x_0 to maximize $(z_k - \hat{z}_k)$ [4, 12].

However, the nature could maximize $(z_k - \hat{z}_k)$ by simply using infinite magnitudes for w_k, v_k and x_0, but this would not make the game fair, as this is not a clever choice. One of the ideas is to put the terms w_k, v_k and x_0 in the denominator and a commonly used cost function is

$$J_1 = \frac{\displaystyle\sum_{k=0}^{N-1} \|z_k - \hat{z}_k\|_{S_k}^2}{\|x_0 - \hat{x}_0\|_{P_0^{-1}}^2 + \displaystyle\sum_{k=0}^{N-1} \left(\|w_k\|_{Q_k^{-1}}^2 + \|v_k\|_{R_k^{-1}}^2 \right)} \tag{17}$$

The notation $\|x_k\|_{S_k}^2$ is defined as the square of the x_k weighted by S_k, or the L_2 norm of x_k, *i.e.*, $\|x_k\|_{S_k}^2 = x_k^T S_k x_k$. The weighting matrices P_0, Q_k, R_k and S_k are symmetric positive definite matrices chosen by the user based on the specific problem.

The direct minimization of J_1 in Eq. (17) is not tractable, so instead we choose a performance bound and seek an estimation strategy that satisfies such threshold. That is, we will try to find an estimate $\hat{z}_k$ that results in

$$J_1 < \frac{1}{\gamma} \tag{18}$$

where $\gamma \geq 0$ is our user-specific performance bound. Rearranging the Eq. (17) results in

$$J = -\frac{1}{\gamma} \|x_0 - \hat{x}_0\|_{P_0^{-1}}^2 + \sum_{k=0}^{N-1} \left[\|z_k - \hat{z}_k\|_{S_k}^2 - \frac{1}{\gamma} \left(\|w_k\|_{Q_k^{-1}}^2 + \|v_k\|_{R_k^{-1}}^2 \right) \right] < 1 \tag{19}$$

where J is defined by the above equation. The minimax problem becomes

$$J^* = \min_{\hat{z}_k} \max_{w_k, v_k, x_0} J \tag{20}$$

Since $v_k = y_k - h(x_k)$, $z_k = L_k x_k$, $\hat{z}_k = L_k \hat{x}_k$ and defining $\bar{S}_k = L_k^T S_k L_k$. Thus, the Eq. (20) can be rewritten as

$$J^* = \min_{\hat{x}_k} \max_{w_k, y_k, x_0} J \tag{21}$$

With the results in Eq. (19) one obtains

$$J = -\frac{1}{\gamma} \|x_0 - \hat{x}_0\|_{P_0^{-1}}^2 + \sum_{k=0}^{N-1} \left[\|x_k - \hat{x}_k\|_{\bar{S}_k}^2 - \frac{1}{\gamma} \left(\|w_k\|_{Q_k^{-1}}^2 + \|y_k - h(x_k)\|_{R_k^{-1}}^2 \right) \right] \tag{22}$$

7

Define $\Psi(\mathbf{x}_0) = -\frac{1}{\gamma}\|\mathbf{x}_0 - \hat{\mathbf{x}}_0\|^2_{\mathbf{P}_0^{-1}}$ and $\mathcal{L}_k = \|\mathbf{x}_k - \hat{\mathbf{x}}_k\|^2_{\bar{\mathbf{S}}_k} - \frac{1}{\gamma}\left(\|\mathbf{w}_k\|^2_{\mathbf{Q}_k^{-1}} + \|\mathbf{y}_k - h(\mathbf{x}_k)\|^2_{\mathbf{R}_k^{-1}}\right)$, J in Eq. (22) becomes

$$J = \Psi(\mathbf{x}_0) + \sum_{k=0}^{N-1}\mathcal{L}_k \tag{23}$$

To resolve of the minimax problem in Eq. (22), a stationary point of J with respect to $\mathbf{x}_0$ and $\mathbf{w}_k$ needs to be found first, and then a stationary point of J with respect to $\hat{\mathbf{x}}_k$ and $\mathbf{y}_k$ needs to be found [12].

4.1. The Second-Order Extended H_∞ Filter Solution

Consider the minimax problem in Eq. (22), using the Taylor series expansion described in Eq. (12) and (13) to approximate the nonlinear function in Eq. (11). The stationary point of J with respect to $\mathbf{x}_0$ and $\mathbf{w}_k$ is given by

$$\mathbf{x}_0 = \hat{\mathbf{x}}_0 + \mathbf{P}_0\boldsymbol{\lambda}_0 \tag{24}$$

$$\mathbf{w}_k = \mathbf{Q}_k\boldsymbol{\lambda}_{k+1} \tag{25}$$

$$\boldsymbol{\lambda}_N = 0 \tag{26}$$

$$\boldsymbol{\lambda}_k = \mathbf{G}_k^{-1}\left[\mathbf{F}_k^T\boldsymbol{\lambda}_{k+1} + \gamma\bar{\mathbf{S}}_k(\boldsymbol{\mu}_k - \hat{\mathbf{x}}_k) + \mathbf{H}_k^T\mathbf{R}_k^{-1}(\tilde{\mathbf{y}}_k - \mathbf{H}_k(\boldsymbol{\mu}_k - \hat{\mathbf{x}}_k))\right] \tag{27}$$

$$\mathbf{P}_{k+1} = \mathbf{F}_k\mathbf{P}_k\mathbf{G}_k^{-1}\mathbf{F}_k^T + \mathbf{Q}_k \tag{28}$$

$$\boldsymbol{\mu}_0 = \hat{\mathbf{x}}_0 \tag{29}$$

$$\begin{aligned}\boldsymbol{\mu}_{k+1} = & \ f(\hat{\mathbf{x}}_k, \boldsymbol{\mu}_k) + \mathbf{F}_k(\boldsymbol{\mu}_k - \hat{\mathbf{x}}_k) + \frac{1}{2}\sum_{i=1}^{n}\varphi_i^f tr\left[\frac{\partial^2 f_i}{\partial \mathbf{x}_k^2}\Big|_{\hat{\mathbf{x}}_k}\bar{\mathbf{P}}_k\right] \\ & + \mathbf{F}_k\mathbf{P}_k\mathbf{G}_k^{-1}\left[\gamma\bar{\mathbf{S}}_k(\boldsymbol{\mu}_k - \hat{\mathbf{x}}_k) + \mathbf{H}_k^T\mathbf{R}_k^{-1}(\tilde{\mathbf{y}}_k - \mathbf{H}_k(\boldsymbol{\mu}_k - \hat{\mathbf{x}}_k))\right]\end{aligned} \tag{30}$$

where

$$\mathbf{F}_k = \frac{\partial f}{\partial \mathbf{x}_k}\Big|_{\hat{\mathbf{x}}_k} \tag{31}$$

$$\mathbf{H}_k = \frac{\partial h}{\partial \mathbf{x}_k}\Big|_{\hat{\mathbf{x}}_k} \tag{32}$$

$$\tilde{\mathbf{y}}_k = \mathbf{y}_k - h(\hat{\mathbf{x}}_k) - \frac{1}{2}\sum_{i=1}^{m}\varphi_i^h tr\left[\frac{\partial^2 h_i}{\partial \mathbf{x}_k^2}\Big|_{\hat{\mathbf{x}}_k}\bar{\mathbf{P}}_k\right] \tag{33}$$

$$G_k = I - \gamma \bar{S}_k P_k + H_k^T R_k^{-1} H_k P_k \tag{34}$$

The proof and the mathematical development can be found in References [4] and [12].

With the results of x_0 and w_k present in Eq. (24) and (25), the stationary point of J with respect to $\hat{x}_k$ and y_k is given by

$$\hat{x}_k = \mu_k \tag{35}$$

$$y_k = h(\hat{x}_k) + \frac{1}{2} \sum_{i=1}^{m} \varphi_i^h tr \left[\left. \frac{\partial^2 h_i}{\partial x_k^2} \right|_{\hat{x}_k} \bar{P}_k \right] \tag{36}$$

The proof and the mathematical development can be found again in References [4] and [12].

However, the Second-Order Extended H_∞ Filter Solution, presented for the space state represented by Eq. (11), is given by combination of the Eq. (30), (28), (35) and (36), thus [12, 4]:

$$\bar{S}_k = L_k^T S_k L_k \tag{37}$$

$$K_k = P_k \left[I - \gamma \bar{S}_k P_k + H_k^T R_k^{-1} H_k P_k \right]^{-1} H_k^T R_k^{-1} \tag{38}$$

$$\hat{x}_{k+1} = f(\hat{x}_k, \mu_k) + \frac{1}{2} \sum_{i=1}^{n} \varphi_i^f tr \left[\left. \frac{\partial^2 f_i}{\partial x_k^2} \right|_{\hat{x}_k} \bar{P}_k \right] + F_k K_k \tilde{y}_k \tag{39}$$

$$P_{k+1} = F_k P_k \left[I - \gamma \bar{S}_k P_k + H_k^T R_k^{-1} H_k P_k \right]^{-1} F_k^T + Q_k \tag{40}$$

$$\lambda_{k+1} = \left(F_k F_k^T + \xi I \right)^{-1} F_k \left(G_k \lambda_k - H_k^T R_k^{-1} \tilde{y}_k \right) \tag{41}$$

$$\bar{P}_{k+1} = \eta \bar{P}_k + (1 - \eta) P_k \lambda_k \lambda_k^T P_k^T \tag{42}$$

where ξ is positive scalar to prevent the term $F_k F_k^T$ from being singular and $0 < \eta \leq 1$. Furthermore, the value of γ must satisfy the Eq. (43) to ensure that the optimized value of $\hat{x}_k$ yields a local minimum of J, *i.e.*

$$P_k^{-1} - \gamma \bar{S}_k + H_k^T R_k^{-1} H_k > 0 \tag{43}$$

That is, the expression, $P_k^{-1} - \gamma \bar{S}_k + H_k^T R_k^{-1} H_k$, must be positive definite.

4.2. The Extended Kalman Filter Solution

In the Extended Kalman Filter, the noises w_k and v_k are assumed to be white, zero mean, and uncorrelated. They are assumed to have known covariance matrices $\tilde{Q}_k$ and $\tilde{R}_k$, respectively [4, 12].

$$E\left[w_k w_k^T\right] = \tilde{Q}_k$$
$$E\left[v_k v_k^T\right] = \tilde{R}_k \tag{44}$$
$$E\left[w_k v_k^T\right] = 0$$

where $E\left[.\right]$ denotes the expectation operation.

The Extended Kalman Filter use the Taylor series expansion described in Eq. (12) and (13), and find the optimal estimate $\hat{x}_k$ that minimizes the estimation error defined as

$$E\left[x_k - \hat{x}_k\right] = 0 \tag{45}$$

The Extended Kalman Filter Solution for the nonlinear function, present in Eq. (11), is given as follows [12].

Time update equations:

$$\hat{x}_k^- = f(\hat{x}_{k-1}^+, \mu_k) \tag{46}$$

$$\tilde{P}_k^- = \tilde{F}_{k-1}\tilde{P}_{k-1}^+\tilde{F}_{k-1}^T + \tilde{Q}_{k-1} \tag{47}$$

Measurements update equations:

$$\hat{x}_k^+ = \hat{x}_k^- + \tilde{K}_k\left(y_k - h(\hat{x}_k^-)\right) \tag{48}$$

$$\tilde{K}_k = \tilde{P}_k^-\tilde{H}_k^T\left(\tilde{H}_k\tilde{P}_k^-\tilde{H}_k^T + \tilde{R}_k\right)^{-1} \tag{49}$$

$$\tilde{P}_k^+ = \left(I - \tilde{K}_k\tilde{H}_k\right)\tilde{P}_k^- \tag{50}$$

where $\tilde{F}_k = \left.\frac{\partial f}{\partial x_k}\right|_{\hat{x}_k^+}$ and $\tilde{H}_k = \left.\frac{\partial h}{\partial x_k}\right|_{\hat{x}_k^-}$.

After some laborious algebraic operations [12], the Kalman gain $\tilde{K}_k$ can be rewritten as the Eq. (51) and the estimation error covariance matrix $\tilde{P}_k^-$ and $\tilde{P}_k^+$ can be integrated and presented as the Eq. (52):

$$\tilde{K}_k = \tilde{P}_k^-\left[I + \tilde{H}_k^T\tilde{R}_k^{-1}\tilde{H}_k\tilde{P}_k^-\right]^{-1}\tilde{H}_k^T\tilde{R}_k^{-1} \tag{51}$$

$$\tilde{P}_{k+1}^- = \tilde{F}_k\tilde{P}_k^-\left[I + \tilde{H}_k^T\tilde{R}_k^{-1}\tilde{H}_k\tilde{P}_k^-\right]^{-1}\tilde{F}_k^T + \tilde{Q}_k \tag{52}$$

4.3. A Comparison between the Second-Order Extended H_∞ Filter and the Extended Kalman Filter

On comparing the Second-Order Extended H_∞ Filter (SOEH_∞F) with the Extended Kalman Filter (EKF), we can observe that the structures of matrices K_k and P_{k+1} in the SOEH_∞F, presented in Eq. (38) and (40), are similar to the matrices $\tilde{K}_k$ and $\tilde{P}_{k+1}^-$ in the EKF, presented in Eq. (51) and (52). If the weighting matrices P_0, Q_k and R_k are the same as the covariance matrices $\tilde{P}_0$, $\tilde{Q}_k$ and $\tilde{R}_k$, then K_k and P_{k+1} have the same structures as $\tilde{K}_k$ and $\tilde{P}_{k+1}^-$, respectively, when $\gamma \to 0$.

In the SOEH_∞F, the Q_k, R_k and P_0 are design matrices chosen by the user based on a *priori* knowledge of the magnitude of the process disturbances w_k, the measurement disturbance v_k, and the initial estimation error $(x_0 - \hat{x}_0)$. In the EKF, the terms w_k, v_k and $(x_0 - \hat{x}_0)$ are zero mean, and Q_k, R_k and P_0 are their respective covariances [12].

Therefore, the SOEH_∞F equations make sense intuitively when compared with the EKF equations. The SOEH_∞F is the worst-case filter in sense that it assumes that w_k, v_k and x_0 will be chosen by nature to maximize the cost function. Comparing the filters, we can see that the SOEH_∞F is simply a robust version of the EKF.

5. Computer Simulation and Results

The nonlinear system that represents the process and measurements equations by the CBERS-2 satellite is given by:

$$
\begin{bmatrix} \dot{\phi} \\ \dot{\theta} \\ \dot{\psi} \\ \dot{\varepsilon}_x \\ \dot{\varepsilon}_y \\ \dot{\varepsilon}_z \end{bmatrix} = \begin{bmatrix} \omega_0 \sin\psi + (g_x - \varepsilon_x) + \theta(g_z - \varepsilon_z) \\ \omega_0 \cos\psi + (g_y - \varepsilon_y) - \phi(g_z - \varepsilon_z) \\ \omega_0 \theta \sin\psi + (g_z - \varepsilon_z) + \phi(g_y - \varepsilon_y) \\ 0 \\ 0 \\ 0 \end{bmatrix} + w \tag{53}
$$

$$
y_k = \begin{bmatrix} \arctan\left(\dfrac{-(S_{0y} - \psi S_{0x} + \phi S_{0z})}{(S_{0x} + \psi S_{0y} - \theta S_{0z})\cos 60 + (S_{0z} - \phi S_{0y} - \theta S_{0z})\cos 150} \right) \\ 24 + \arctan\left(\dfrac{S_{0x} + \psi S_{0y} - \theta S_{0z}}{S_{0z} - \phi S_{0y} - \theta S_{0z}} \right) \\ \phi \\ \theta \end{bmatrix} + v_k \tag{54}
$$

Remembering that the state vector is composed by the attitude angles ϕ, θ, ψ, and by gyros bias ε_x, ε_y, ε_z; and the term ω_0 is an angular velocity that represents the orbital rate of the navigation in relationship to Earth. The terms g_x, g_y ans g_z are the components of the gyroscope output vector; the matrices $w = \begin{bmatrix} w_\phi & w_\theta & w_\psi & w_{\varepsilon_x} & w_{\varepsilon_y} & w_{\varepsilon_z} \end{bmatrix}^T$ and $v_k = \begin{bmatrix} v_{\alpha_\psi} & v_{\alpha_\theta} & v_{\phi_H} & v_{\theta_H} \end{bmatrix}^T$ are the

process and measurements noises, respectively; and the terms S_{0x}, S_{0y} and S_{0z} are the components of the solar vector in orbital coordinate system.

To validate and analyze the performance of estimators, actual sensors data of CBERS-2 satellite, launched on October 21, 2003, were used. The measures are for the day April 21, 2006, being collected by the ground system at a sampling rate of about 8.56s for about 10 min of observation from 13h46min25s until 13h55min27s. To easy, the graphical represention of measurements of the sensors DSS and IRES in Fig. 3 and measures of the gyroscope in Fig. 4, are shown below.

Figure 3. Graphical representation of DSS and IRES real data of CBERS-2 satellite
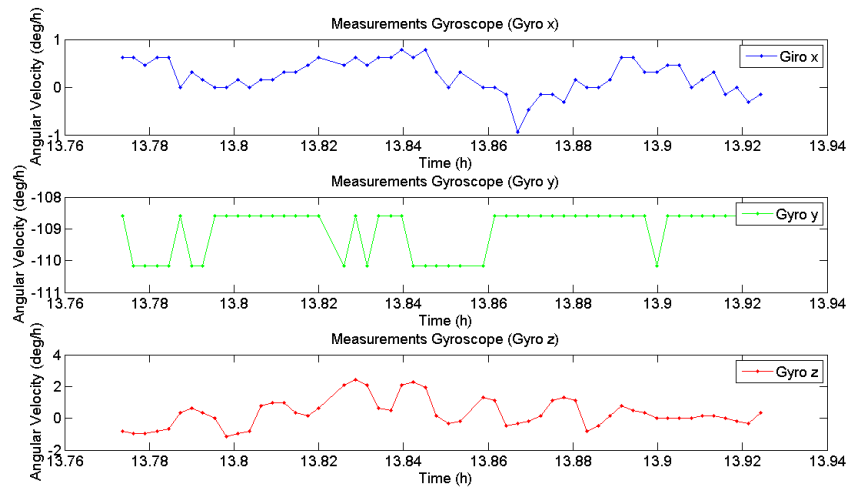

Figure 4. Graphical representation of gyros real data of CBERS-2 satellite

In fact, the ACS (Attitude Control System) on board the satellite has full access to sensor measurements sampled at a rate of 4Hz for the three gyros, aligned with axes *x*, *y* and *z* of the satellite; 1Hz for the two Infrared Earth Sensors to the angle ϕ (*roll*) and θ (*pitch*); and 0.25Hz for both Digital Solar Sensors, related to the angles of *pitch* (α_θ) and *yaw* (α_ψ) [13].

12

The algorithm of the state estimation by the Second-Order Extended H_∞ Filter was coded in MatLab sofware. The initial conditions used were $\boldsymbol{x}_0 = \begin{bmatrix} 0.0 & 0.0 & 0.0 & 5.76 & 4.64 & 2.68 \end{bmatrix}^T$; the covariance matrix $\boldsymbol{P}_0 = diag\,(0.25;0.25;4.0;1.0;1.0;1.0)$; the process and measurements error matrix, $\boldsymbol{Q}_0 = diag\,(0.01;0.01;0.01;10^{-4};10^{-4};2.5 \times 10^{-5})$ and $\boldsymbol{R}_0 = diag\,(0.36;0.36;0.0036;0.0036)$, respectively; the auxiliar covariance matrix $\bar{\boldsymbol{P}}_0 = diag\,(0.25;0.25;4.0;1.0;1.0;1.0)$ and initial Lagrange multiplier $\boldsymbol{\lambda}_0 = \begin{bmatrix} 0.1 & 0.1 & 0.1 & 0.1 & 0.1 & 0.1 \end{bmatrix}^T$. For the vector $\boldsymbol{x}_0$, the first three elements are in deg and the others elements are in deg/h, for the matrices $\boldsymbol{P}_0$, $\boldsymbol{Q}_0$ and $\bar{\boldsymbol{P}}_0$ the first three elements are in deg^2 and the others elements are in deg^2/h^2, and finally, for the matrix $\boldsymbol{R}_0$ all the elements are in deg^2.

The Figures 5, 6 and 7, present the attitude angles and gyros bias estimation using the EH_∞F, the SOEH_∞F and the EKF. It is important to emphasize that the state estimation by EKF was used as a reference [8]. For the SOEH_∞F, the parameters used were $\gamma = 1/3$, $\eta = 0.9$, $\xi = 1.3$ and the matrices L_k and S_k are both set to be identity matrices.
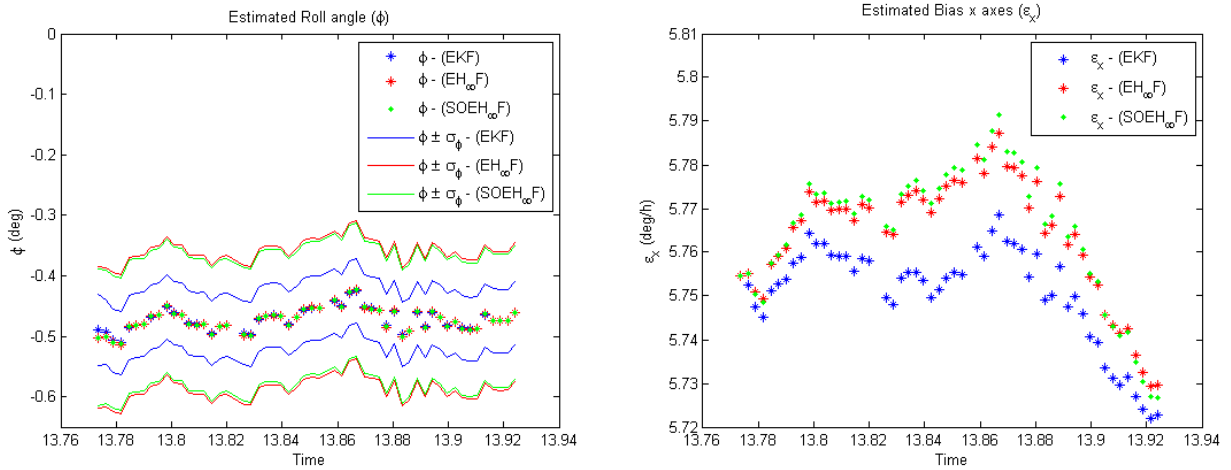

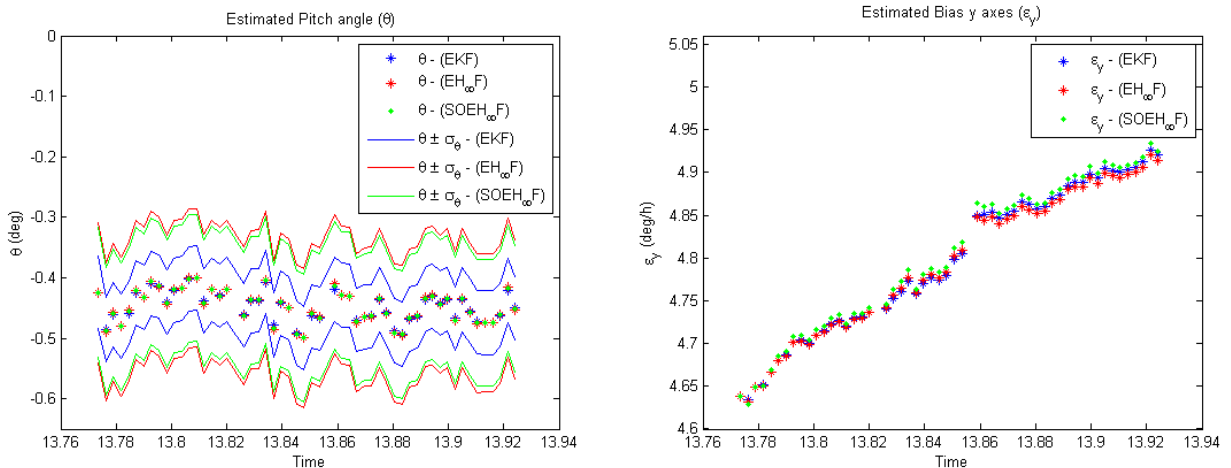**Figure 5. Estimated *roll* angle and bias gyro around the x axis**

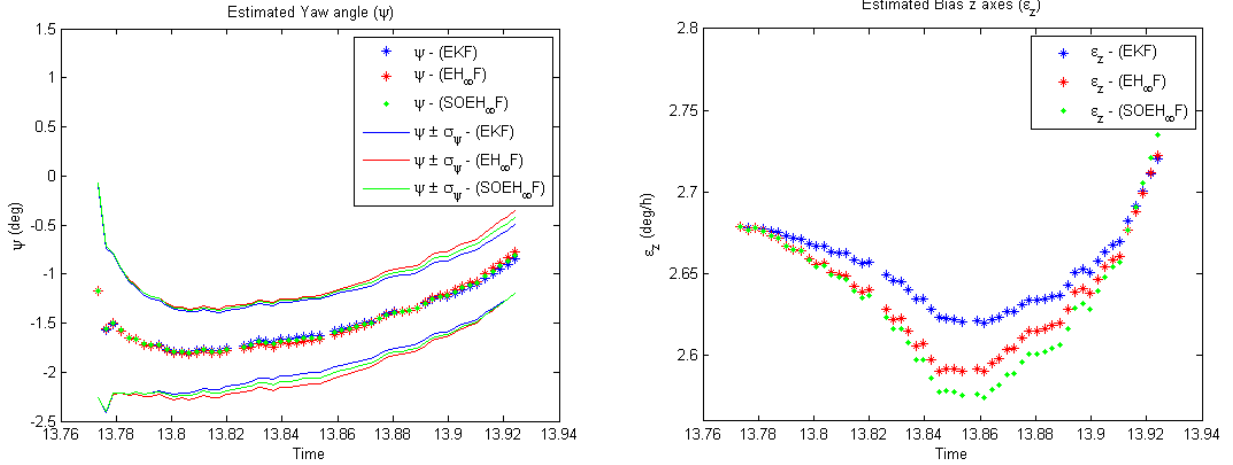**Figure 6. Estimated *pitch* angle and bias gyro around the y axis**

13

Figure 7. Estimated *yaw* angle and bias gyro around the z axis

By the behavior of *roll* and *pitch* angle estimated (Fig. 5 and 6 left, respectively) it is observed that the SOE*H*∞F produces satisfactory results according to the reference, but with higher standard deviation. The behavior of bias gyro estimated around the **x** axis (Fig. 5 right) present a smooth deviation, but consistent with the reference results. However, the behavior of bias gyro estimated around the **y** axis (Fig. 6 right) present similar results to the reference. Finally, the behavior of *yaw* angle estimated (Fig. 7 left) it is observed that the SOE*H*∞F present similar results to the reference. The behavior of bias gyros estimated around the **z** axis (Fig. 7 right) present smooth deviation but again consistent with the reference.

In Figures 8 and 9 present the standard deviation of attitude angles and standard deviation of the gyros bias, respectively, by the E*H*∞F, the SOE*H*∞F and the EKF.
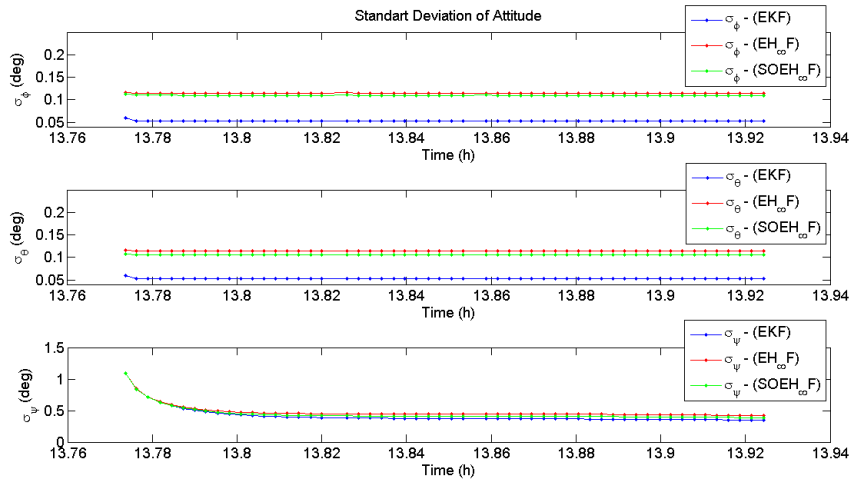

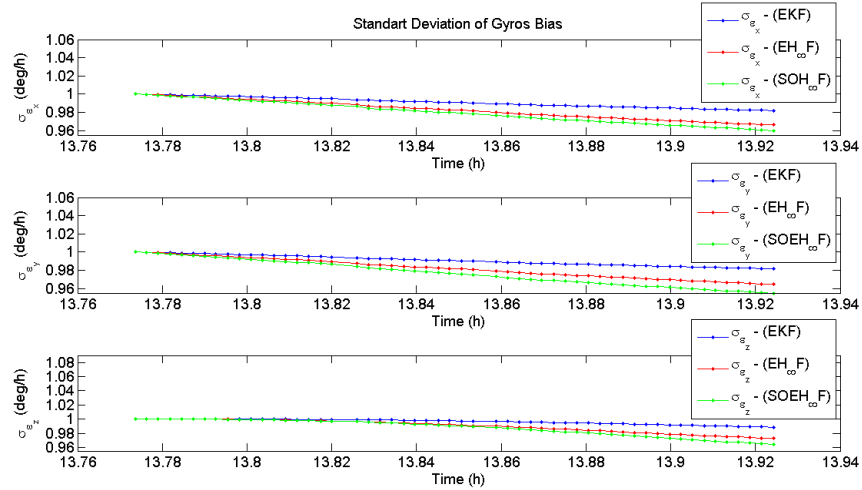**Figure 8. Standard deviation of attitude angles**

14

Figure 9. Standard deviation of gyros bias

Analyzing the results, it is observed that the standard deviation of attitude angles are higher in the SOEH_∞F and EH_∞F than in the EKF. The standard deviation of gyros bias covariance in the SOEH_∞F and EH_∞F present better results than EKF because goes to smaller values quicker. Thus, for the gyros calibration the SOEH_∞F provides more reliable results.

The following, in Fig. 10 and 11, presented the residuals of the two Digital Solar Sensor (DSS) and of the two Infrared Earth Sensor (IRES) by the SOEH_∞F, the EH_∞F and the EKF, which are quite similar.
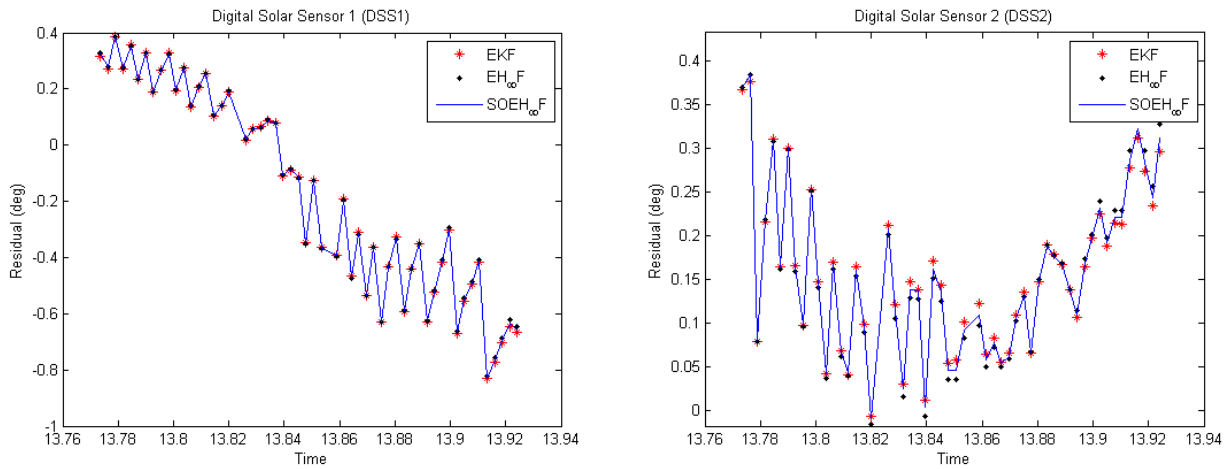

Figure 10. Residuals of the two DSS on board the CBERS-2 satellite

It is known that the convergence of a Filter is reflected in the residual results which must oscillate around zero. Analyzing the Fig. 10 and 11 it is observed that the IRES1 and IRES2 residual show the espected behavior but DSS1 e DDS2 residual are skewed. This result is due to a small delay in the sensors measurements time tagging, which is misplaced.
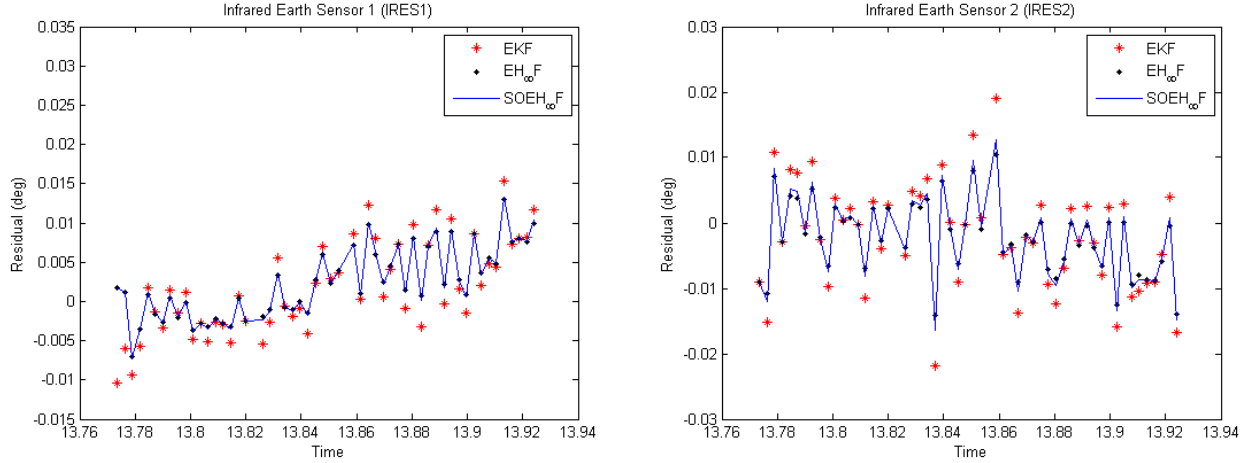
15

Figure 11. Residuals of the two IRES on board the CBERS-2 satellite

6.   Conclusions

The usage of real data from on board attitude sensors, poses difficulties like mismodelling, mismatch of sizes, misalignments, unforeseen systematic errors and post-launch calibration errors. However, it is observed that the attitude estimated by the SOE*H*∞F are in close agreement with the results in previous works [8, 9] which used the EKF for attitude estimation.

Regarding the robustness of the estimation method SOE*H*∞F, it was noted that the results are similar with the reference EKF but the gyros bias covariance by the SOE*H*∞F provides results supposedly more accurate for gyros calibration.

According to the theory, the weighting matrices $\boldsymbol{Q}_k$, $\boldsymbol{R}_k$ and $\boldsymbol{S}_k$ in SOE*H*∞F are symmetric positive definite matrices which can be designed by the user without requiring them to be diagonal, but the noise covariance matrices $\tilde{\boldsymbol{Q}}_k$ and $\tilde{\boldsymbol{R}}_k$ in EKF are normally set to be diagonal. However, different weighting matrices result in different performance [12].

It is noted that, the SOE*H*∞F can be more robust to the unmodeled noise than the EKF when the weighting matrices $\boldsymbol{Q}_k$ and $\boldsymbol{R}_k$ are the same to the covariance matrices $\tilde{\boldsymbol{Q}}_k$ and $\tilde{\boldsymbol{R}}_k$ of the EKF. The SOE*H*∞F is a worst-case filter in the sense that it assumes that the process and measurements noises, $\boldsymbol{w}_k$ and $\boldsymbol{v}_k$ respectively, and the initial condition $\boldsymbol{x}_0$ will be chosen by nature to maximize the cost function. Comparing these filters, we can infer that the SOE*H*∞F is simply a robust version of the EKF.

Finally, it can be concluded that the algorithm of the SOE*H*∞F converges, providing a kinematic attitude solution besides estimating biases (gyro drifts) with superior accuracy as compared with the EKF.

7. Acknowledgment

8. References

[1] Banavar, R. "A game theoretic approach to linear dynamics estimation.", 1992.

[2] Shen, X. and Deng, L. "Discrete H_∞ filter design with application to speech enhancement." IEEE International Conference on Acoustics, Speech and Signal Processing, Vol. 2, pp. 1504 – 1507, 1995.

[3] Shen, X. and Deng, L. "Game theory approach to H_∞ discrete filter design." IEEE Transactions on Signal Processing, pp. 1092 – 1094, 1997.

[4] Hu, J. S. and Yang, C. H. "Second-Order Extended H_∞ Filter for Nonlinear Discrete-Time Systems Using Quadratic Error Matrix Approximation." IEEE Transactions on Signal Processing, Vol. 59, No. 7, pp. 3110 – 3119, 2011.

[5] Silva, W. R., Zanardi, M. C., Cabette, R. E. S., and Formiga, J. K. S. "Study of stability of rotational motion of spacecraft with canonical variables." Mathematical Problems in Engeneering, Vol. 2012, pp. 1 – 19, 2012.

[6] Fuming, H. and Kuga, H. K. "CBERS simulator mathematical models." CBTT Project, CBTT/ 2000/ MM/ 001, 1999.

[7] Wertz, J. R. Spacecraft attitude determination and control. D. Reidel, Dordrecht, Holanda, 1978.

[8] Garcia, R. V., Kuga, H. K., and Zanardi, M. C. "Unscented Kalman filter applied to the spacecraft attitude estimation with euler angles." Mathematical Problems in Engineering, Vol. 2012, pp. 1–12, 2012.

[9] Garcia, R. V., Kuga, H. K., and Zanardi, M. C. "Unscented Kalman filter for spacecraft attitude estimation using quaternions and euler angles." 22nd International Symposium on Space Flight Dynamics, 2011.

[10] Crassidis, J. L. and Markley, F. L. "Unscented filtering for spacecraft attitude estimation." Journal of Guidance, Control and Dynamics, Vol. 26, No. 4, pp. 536 – 542, 2003.

[11] Lefferts, E. J., Markley, F. L., and Shuster, M. D. "Kalman filtering for spacecraft attitude estimation." Journal of Guidance, Vol. 5, No. 5, pp. 417 – 429, 1982.

[12] Simon, D. Optimal State Estimation: Kalman, H_∞, and Nonlinear Approaches. Wiley, New York, 2006.

[13] Lopes, R. V. F. and Kuga, H. K. "CBERS-2: On Ground Attitude Determination From Telemetry Data." INPE, Internal Report C-ITRP, 2005.